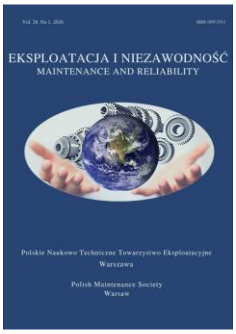

Eksploatacja i Niezawodnosc – Maintenance and Reliability
Volume 28 (2026), Issue 1
journal homepage: http://www.ein.org.pl

Article citation info:
Wang J, Abdullah S, Arifin A, Singh S, S, K, Gao C, A Semi-supervised Fault Diagnosis Method for Rolling Bearing Using Time-Frequency Transform Enhanced Contrastive Learning, Eksploatacja i Niezawodnosc – Maintenance and Reliability 2026: 28(1) http://doi.org/10.17531/ein/207015

Indexed by:

A Semi-supervised Fault Diagnosis Method for Rolling Bearing Using Time-Frequency Transform Enhanced Contrastive Learning

Jicai Wang[a,b], Shahrum Abdullah[b,*], Azli Arifin[b], Salvinder Singh Karam Singh[b], Chen Gao[a,b,*]

[a] School of Electromechanical and Transportation, Jiaxing Nanyang Polytechnic Institute, China
[b] Department of Mechanical and Manufacturing Engineering, Universiti Kebangsaan Malaysia, Malaysia

Highlights

- A semi-supervised learning method for bearing fault diagnosis was proposed.
- A STFT enhanced Contrastive Learning is employed to utilize large unlabeled samples.
- The diagnostic accuracy exceeded 99% when using 50 labeled samples per fault type.

Abstract

This paper proposes a novel semi-supervised framework, time-frequency Contrastive Learning (CL), to address the challenge of accurate rolling bearing fault diagnosis under industrial small-sample conditions. Raw vibration signals are transformed into discriminative time-frequency images using short-time Fourier transform (STFT). A CL network with a ResNet18 model is pre-trained on a lot of unlabeled samples to learn generalized feature, and the ResNet18 model is fine-tuned using small labeled samples for fault classification. Experimental validation on bearing fault datasets demonstrates that the proposed STFT-CL method achieves above 99% diagnosis accuracy with only 50 labeled samples per fault type, outperforming conventional semi-supervised methods by 6-12%. The proposed method provides a potential solution to the "small sample dilemma" in industrial applications through the synergistic effect of physically driven signal processing and self supervised representation learning.

Keywords
rolling bearing, fault diagnosis, semi-supervised learning, time-frequency transform, contrastive learning

1. Introduction

Rolling bearings are precision components that provide support to mechanically rotating bodies. These elements reduce friction coefficients during motion and minimize frictional losses between various mechanical components in the system[1]. However, during actual system operation, the bearings can be damaged due to fatigue resulting from prolonged periods of overload or improper maintenance. Generally, rolling bearings failures account for a large share of failures in power systems. According to reported data, bearing failures in induction motors constitute around 42% of the total number of failures[2]. Therefore, developing and implementing intelligent methods for fault diagnosis of bearings can extend machine operation safety and enhance the system performance and overall efficiency[3-5].

In recent years, a number of deep learning (DL) -based methods were widely used in various applications, demonstrating significant potential for diagnosing faults in rotating machinery[6-12]. DL methods realize end-to-end learning by hierarchically representing and extract high-level representations from low-level features. This effectively

(*) Corresponding author.
E-mail addresses: J. Wang 45154343@qq.com, S. Abdullah shahrum@ukm.edu.my, A. Arifin azli@ukm.edu.my, S. S. K. Singh salvinder@ukm.edu.my, C. Gao (ORCID: 0000-0001-6807-5998) gaochen_1993@163.com

reduces the dependency on data as experienced in traditional machine learning models and algorithms[13-16]. For instance, Wang et al. implemented a convolutional neural networks (CNN) based hidden Markov model to address the mechanical fault classification problem[17]. In a connected work, Anil et al. introduced a novel CNN to improve the fault diagnosis accuracy for bearings. They presented a triangular cross-entropy function to calculate sparsity costs[18]. Zhao et al. developed a convolutional bidirectional long short-term memory (LSTM) network to process raw sensing data to form a basis for machine health monitoring[19]. Also, Chen et al. presented a multi-task network deep domain adaptive model for planetary gearbox fault diagnosis[20]. Zhou et al. proposed a deep kernel based extreme learning machine (KELM) algorithm for predicting milling tool wear values that could improve significantly the performance of tool wear condition monitoring[21]. However, it is noted that these DL-based methods require a lot of labeled samples for training and learning[22-24]. This is challenging in many practical industrial scenarios and creates major problems hindering implementation due to the need for extensive experimentation.

In many actual scenarios, it is difficult to collect sufficient training samples constrained by time and monetary costs, in addition to a large number of unlabeled samples. This situation affects significantly the learning effectiveness of supervised DL models[2526]. On this basis, there is a need to develop a classification method capable of learning from small labeled samples along with large unlabeled samples. Zhou et al. proposed a novel semi-supervised method based on multiscale permutation entropy, in which unlabeled samples could be utilized to extract fault features[27]. This method provides a very novel and effective framework for fault diagnosis in the industrial reality of "small sample, big data", effectively overcoming the problem of fault diagnosis under small sample. It is worth noting that this method requires parameter optimization to obtain the best two-dimensional samples, resulting in high professional requirements for employees.

It is necessary to develop a method that is easy for ordinary employees with weak professionalism to understand and operate. Therefore, this paper establishes a simpler and more feasible method based on time-frequency transform enhanced contrastive learning that can obtain highly accurate performance using small labeled samples and large unlabeled samples. The contributions of this paper are as follows:

(1) A semi-supervised learning method for bearing fault diagnosis has been proposed, which significantly reduces the requirement of deep learning models for a large number of labeled samples by learning features from a large number of unlabeled samples.

(2) A STFT enhanced CL method is proposed, in which STFT is used to enhance the information of samples, while CL learns deep features from unlabeled samples.

(3) The diagnostic accuracy of the proposed method exceeded 99% when using 50 labeled samples per fault type, significantly reducing the dependence of fault diagnosis on sample size.

2. Proposed method

2.1. Contrastive learning

In their research on unsupervised classification, Hardsel et al. introduced contrast loss, which maps high-dimensional data to a low-dimensional space[28]. By calculating the contrast loss of positive pairs and negative pairs, this approach brings similar points closer together in space. In a connected study, Chen et al. developed a contrastive learning (CL) framework, which adds multiple fully connected layers and activation layers after the feature extraction network[29]. In this regard, the model addresses the slow computation speed when considering high-dimensional feature vectors, and good results were reported. Overall, CL has addressed some issues of conventional approaches, including data sparsity and the long-tail distribution of items in recommendation systems[30]. It also showed good performance in natural language processing[3132]. In such applications, the method utilizes data augmentation to bring closer the results of the same sentence after augmentation, as positive examples, in addition to separating different sentences or augmentations of different sentences, as negative examples. Generally, it was shown that the trained model performs well in downstream tasks, such as sentence transformation.

Figure 1 presents the overall framework of CL. The framework includes three modules: data augmentation, feature extraction, and contrastive loss optimization modules.

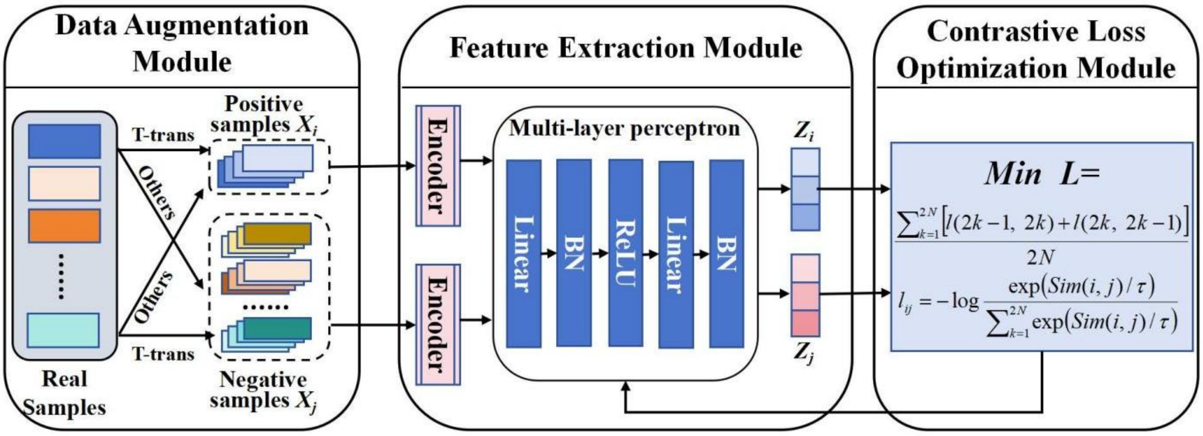

Figure 1. Framework of contrastive learning model.

(1) Data Augmentation Module

Generally, it can augment image through two ways. The first way involves spatial geometric transformations, such as horizontal flipping, vertical flipping, and cropping. The second way involves appearance transformations, such as color jittering and grayscale generation. By default, a set of images obtained through the **T** transform of an image are called positive samples of the original image. On the other hand, paired samples, which are generated from other images, serve as negative samples for this image.

(2) Feature Extraction Module

Feature extraction is performed to obtain feature vectors to serve as inputs for the DL classification model. Here, the multi-layer perceptron (MLP) is applied to extract features. After the first linear layer is normalized, the ReLU function is implemented to explore the relevant features and accelerate the fitting of training data. This allows for speeding up computations in the subsequent loss function calculations[33].

(3) Contrastive Loss Optimization Module

In this module, a batch size of N is specified, where N images are transformed using a **T** transformation. This results in images denoted as N_1 and N_2. The low-dimensional features obtained through the MLP-based feature extraction module are represented as Z_1 and Z_2, respectively, with $Z = [Z_1; Z_2] \in R^{2N\times K}$. In this regard, K denotes the length of the feature vectors Z_1 and Z_2, and $[Z_1; Z_2]$ represents the column-wise concatenation of Z_1 and Z_2. Additionally, the cross-entropy loss of the *i-th* sample can be calculated by using Eq. (1) [29].

$$l_{ij} = -\,log\frac{exp(Sim(i,j)/\tau)}{\sum_{k=1}^{2N} exp(Sim(i,j)/\tau)}, \quad Sim(i,j) = \frac{Z_i^T Z_j}{|Z_i||Z_j|} \tag{1}$$

Where *Sim(i,j)* denotes the cosine similarity function, and $\tau \in [0,1]$ is the temperature coefficient which is used to adjust the focus on hard samples. It is worth noting here that a smaller τ triggers the model towards separating the sample from other similar samples. In Eq. (1), the numerator represents the cosine similarity of positive sample pairs in the *i-th* sample, and the denominator is the sum of the cosine similarities between the *i-th* image and all other samples. According to the findings reported in the literature 29, it was demonstrated that the performance deteriorates significantly without a regularization adjustment and with no inclusion of the τ. Finally, the average of losses L for batch n can be calculated through Eq. (2)[29].

$$L = \frac{1}{2N}\sum_{k=1}^{2N}[l(2k-1,\ \ 2k) + l(2k,\ \ 2k-1)] \tag{2}$$

2.2. Short time Fourier transform (STFT)

In general, STFT is commonly used to analyze time-varying and non-stationary signals. This transformation approach is capable of elevating a one-dimensional signal into a two-dimensional matrix. The latter is easier to process by DL and comprises the spectro-temporal characteristics of the signal[34]. Additionally, the Fourier transform (FT) reflects the overall characteristics of an image, and its frequency domain analysis exhibits good local properties. STFT is developed based on FT, and it is adopted in this study as applying FT directly to the entire process would lead to losing time information[35][36]. On this basis, it is necessary to segment a time-varying and non-stationary signal into multiple stationary signals. To perform this, one approach is to multiply a function by a window function, followed by a 1-D FT. Sliding the window function results in a series of spectral functions, which are then concatenated sequentially to form a two-dimensional spectrogram. This fundamental operation is represented by Eq. (3), where *x(t)* denotes the time-domain signal, *h(t-w)* represents the window function, and ω is its center position[37].

$$STFT_x(t,\omega) = \int_{-\infty}^{+\infty} x(t)h(t-\omega)e^{-jwt}dt \quad (3)$$

2.3. Proposed method procedure

The proposed method includes four steps, as illustrated in Figure 2.

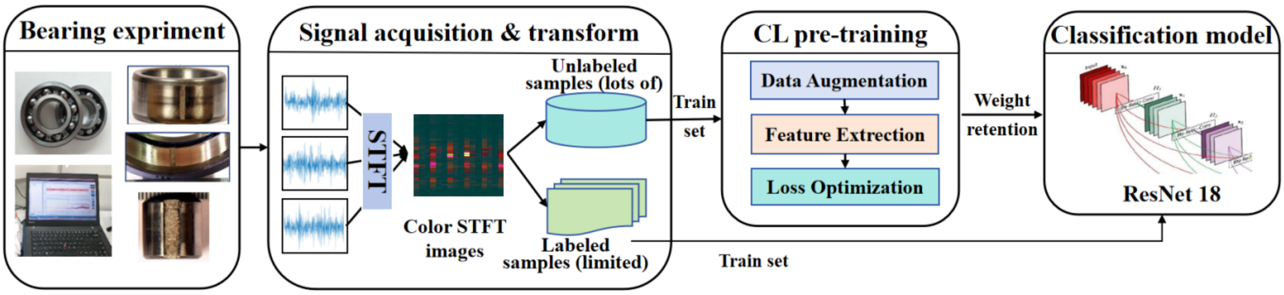

Figure 2. Process of the proposed STFT-CL method.

Step 1: An experimental platform for rolling bearings is established, with parameters configured to replicate real-world operational conditions. A subset of bearings is randomly selected and manually damaged to varying degrees across critical components (e.g., inner/outer rings, rollers) to simulate realistic fault scenarios. This process yielded a dataset comprising limited labeled samples and extensive unlabeled data.

Step 2: The STFT is performed on all collected one-dimensional signals to obtain spectrograms. These spectrograms are then converted to grayscale images. Then, the grayscale images originated from multiple channels are merged to obtain color images.

Step 3: The generated color images in Step 2, which correspond to a large number of unlabeled samples, are introduced to the CL pre-training network to train the network feature weights.

Step 4: The trained feature weights in Step 3 are then used as the initial values for the feature weights of ResNet18. In this process, a few labeled samples are used to fine-tune the ResNet18 model. The trained ResNet18 can then be used for fault diagnosis.

3. Experimental investigation

3.1. Bearing experimental dataset

The setup of the rolling bearing fault diagnosis experiments is shown in Figure 3 [1838]. In the testing system, the geometric specifications of rolling bearings used for fault detection are shown in Table 1. A 346-watt AC motor is employed to deliver power to the shaft through a step pulley mechanism. A 2 kg disc is added in the middle of the shaft, between bearings 1 and 2. This disc rotates with the shaft, and a lever mechanism is utilized to provide a vertical load. To measure this applied load, a load cell is placed below the test bearing housing. Additionally, proximity sensors placed on the test rig record the shaft speed, and a tri-axial accelerometer is used to measure the vibration signals in X, Y, and Z directions at the top of the bearing testing setup. Sampling frequency is 70 kHz.

Table 1. Parameters of experimental bearings [38].

Parameter	Value
Inner ring diameter	25mm
Outer ring diameter	52mm
Pitch diameter	38.9mm
Roller diameter	7.5 mm
Number of rollers	13N
Contact angle	0°

Furthermore, the fault diagnosis experiment on the roller bearing was running at a speed of 2050 rpm while the vertical load is set to 200 N. Using electrical discharge machining (EDM) technology, four different types of wear faults were generated on the inner ring, outer ring, and roller parts, resulting in a total of twelve types of faults. Among them, the inner ring fault size includes four types: 0.43, 1.01, 1.56, and 2.03mm, the outer ring fault size includes four types: 0.42, 0.86, 1.55, and 1.97mm, and the roller fault size includes four types: 0.49, 1.16, 1.73, and

2.12mm, as shown in Figure 4.

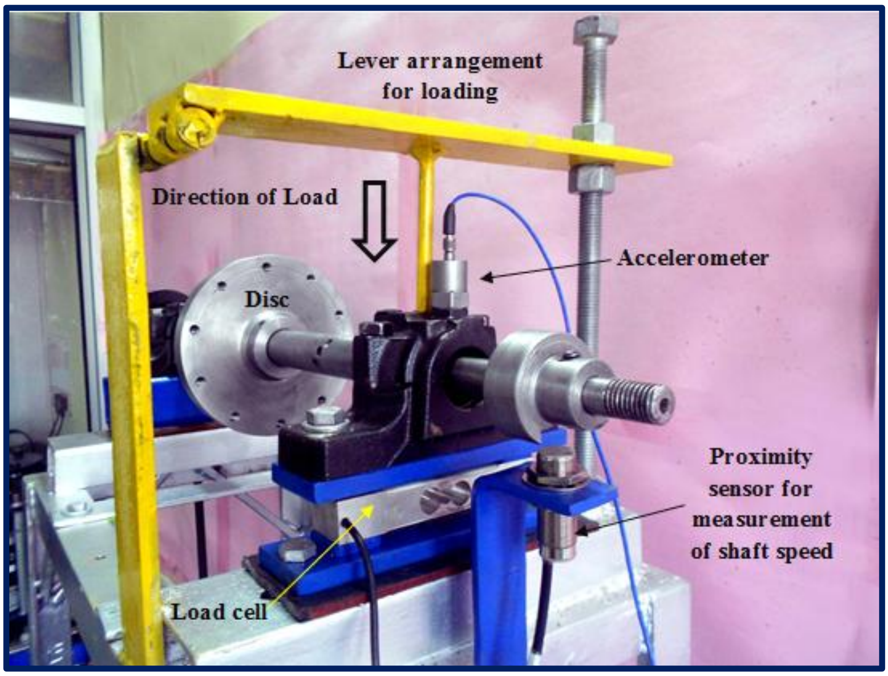

Figure 3. Operation image of the testing bench setup[38].

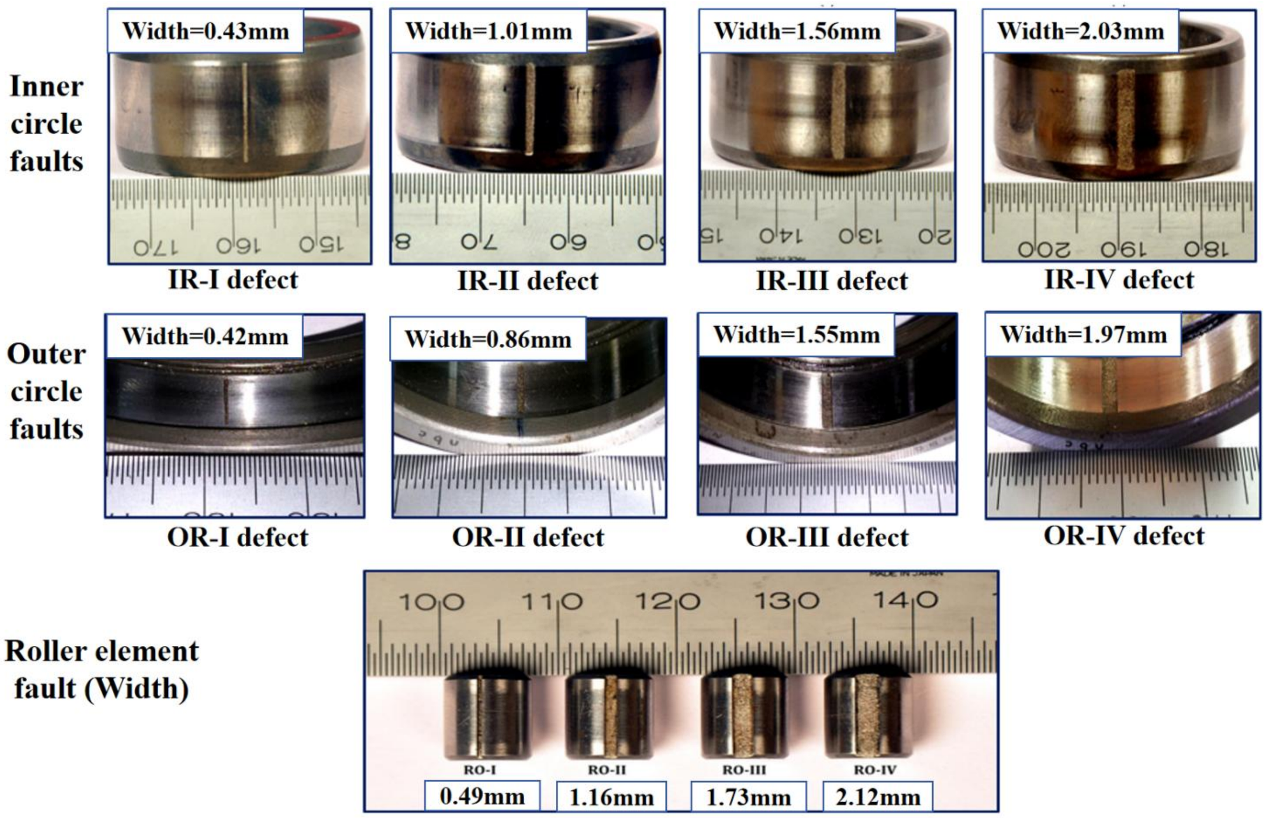

Figure 4. Pictures of twelve fault types.

3.2. Experiment Data Acquisition and Partitioning

Based on these conducted experiments, thirteen bearing conditions, 1 normal condition and 12 fault conditions, were sampled for one cycle period, with each having 2048 points. Three directional (X, Y, and Z) vibration signals were transformed using STFT with a window length of 256 to generate time-frequency grayscale images. The obtained grayscale images from the three channels were then merged into color images, as shown in Figure 5.

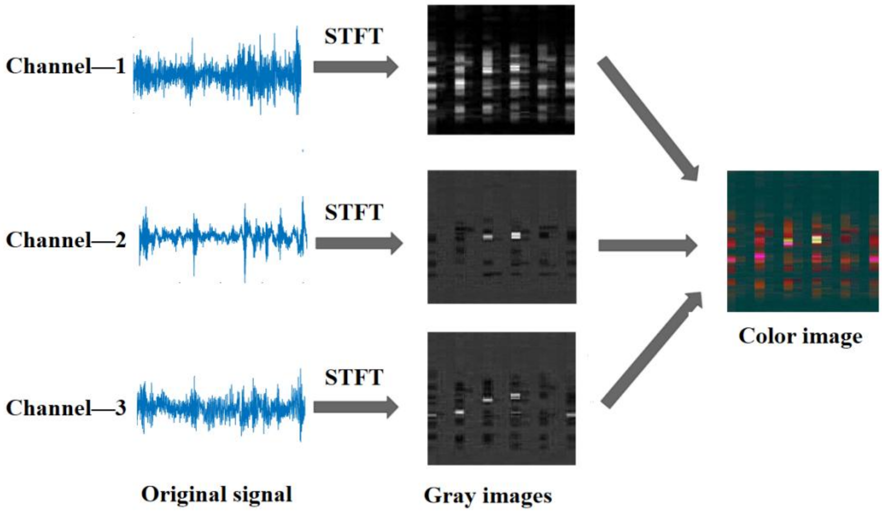

Figure 5. Construction of graphical samples.

Figure 6 to Figure 8 present the color spectrograms generated by STFT for three types of faults: inner race, outer race, and rolling element faults across 12 fault conditions, respectively. Overall, each fault condition produced 1000 graphical samples, resulting in a dataset of 13,000 graphical samples.

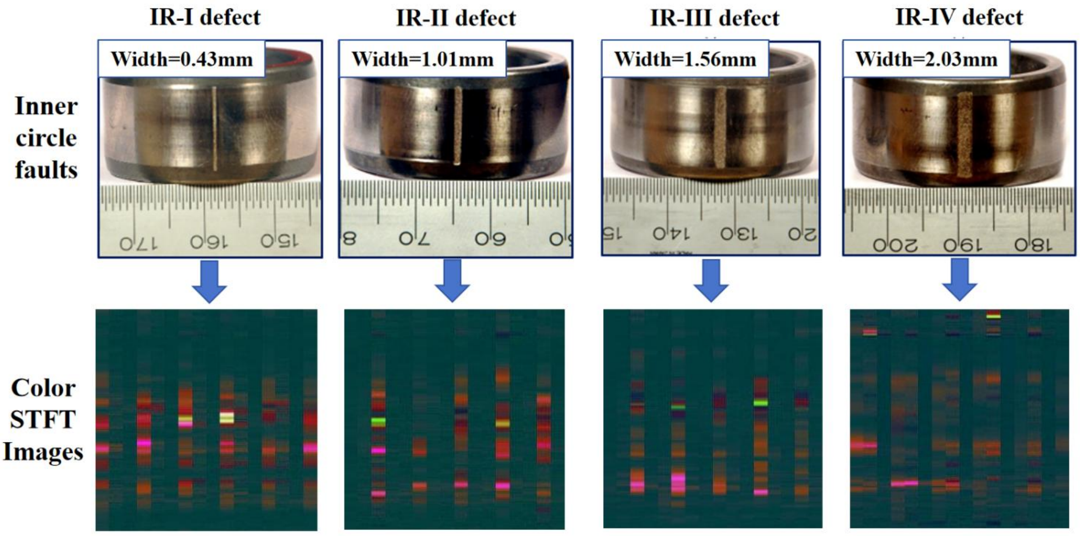

Figure 6. Inner circle faults and their corresponding STFT images.

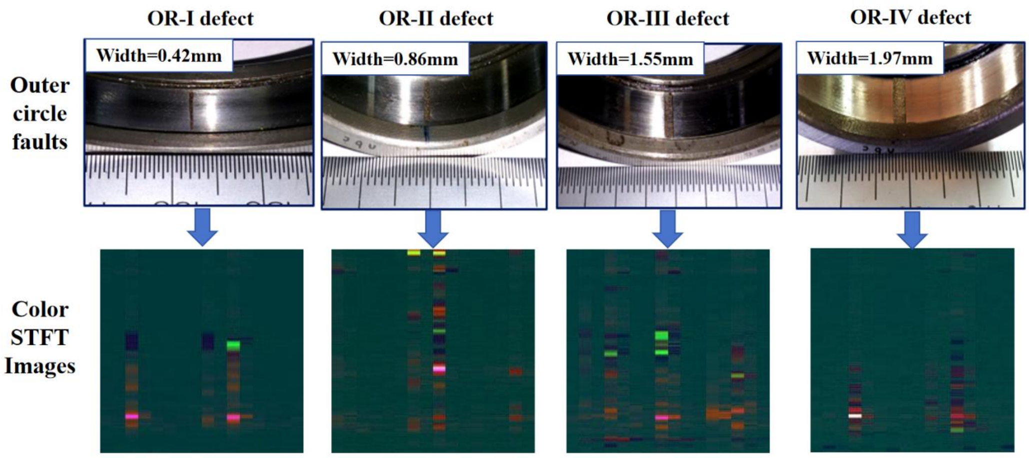

Figure 7. Outer circle faults and their corresponding STFT images.

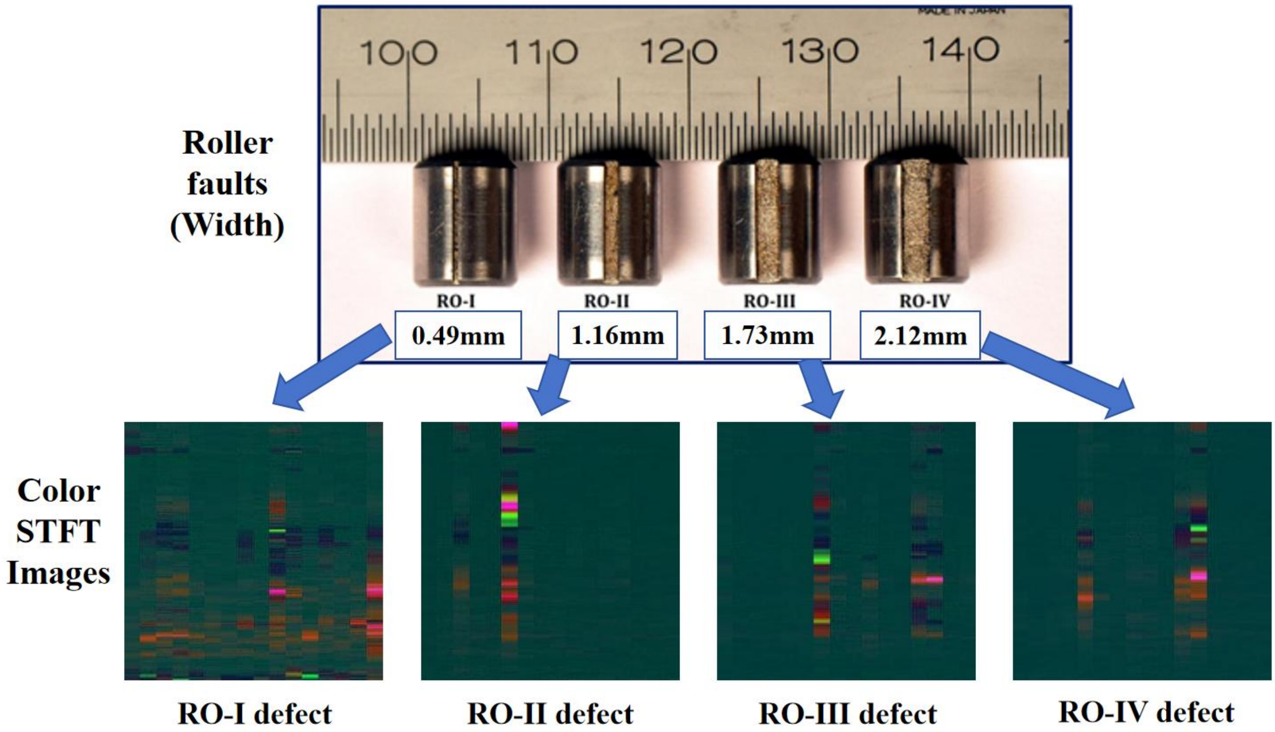

Figure 8. Roller faults and their corresponding STFT images.

Following dataset construction, the samples were partitioned into training and testing sets at an 8:2 ratio, corresponding to 800 and 200 samples, respectively. Within the training set, 650 samples were randomly selected as unlabeled samples to pre-train the CL model, while the remaining 150 labeled samples were reserved for fine-tuning the ResNet18 classification model. The testing set comprised 200 samples per category to ensure comprehensive evaluation. To evaluate the influence of training sample size on diagnostic performance, subsets of labeled data—containing 20, 30, 50, 100, and 150 samples per category—were extracted from the training set. These subsets, designated as TR20, TR30, TR50, TR100, and TR150, were utilized to quantify classification accuracy under varying sample sizes.

3.3. Experimental Results and Analysis

According to articles [22] and [27], the model parameters of the CL pre-training network and the Resnet18 classification model are presented in Table 2. The contrastive loss and CrossEntropy loss functions were employed in the CL pre-training network and the Resnet18 model, respectively. Additionally, the results obtained from the ten repeated experiments using different training sets employing the STFT-CL, STFT-ImageNet pre-training, and STFT-Resnet18 (without pre-training) methods were averaged.

Table 2. Parameters of the CL pre-training and Resnet18 model.

Model	Parameter value				
	Image size	Learning rate	Temperature parameter	Batch size	Optimizer
CL	64×64×3	0.0005	0.1	——	Adam
Resnet18	64×64×3	0.001	——	64	Adam

Table 3 presents the average classification results obtained from ten experiments on five different sample size datasets employing the three methods investigated in this work. It is observed that transforming the signal into time-frequency spectrograms (STFT) to train the model yields consistently high classification accuracies. In this regard, the accuracy exceeds 90% as early as the case considering T-20 samples, while reaching over 98% for all methods in the case of T-150 samples. Overall, it is noted that the proposed CL method obtains higher accuracy compared to other two strategies (IM and Resnet18). In particular, the CL approach exhibited a 2% improvement under STFT with only 20 samples per category in the training dataset.

Table 3. Classification results with different sample sizes.

No.	Labeled/class	Unlabeled/class	Test size/class	STFT-Resnet18	STFT-IM	STFT-CL
T-20	20	650	200	91.82%	92.53%	94.13%
T-30	30	650	200	94.66%	96.37%	96.94%
T-50	50	650	200	97.85%	98.56%	99.04%
T-100	100	650	200	99.29%	99.53%	99.73%
T-150	150	650	200	99.50%	99.73%	99.89%

Furthermore, the confusion matrix of the classification results for the T-20 dataset is illustrated in Figure 9. Here, Label 1 represents the normal condition, Labels 2 to 5 represent different degrees of rolling element faults with increasing wear width, Labels 6 to 9 represent different degrees of inner circle faults with increasing wear width, and Labels 10 to 13 represent different degrees of outer circle faults with increasing wear width. Based on the matrix results, it can be concluded that the model demonstrates high accuracy in identifying the normal condition, inner circle faults, and outer circle faults. However, for rolling element faults, especially the middle two categories, a decrease in the recognition capability of the model is reported. This may be attributed to the rolling elements' ability to both rotate and revolve during operation. Thus, it is more challenging to distinguish these faults compared to inner and outer circle faults.

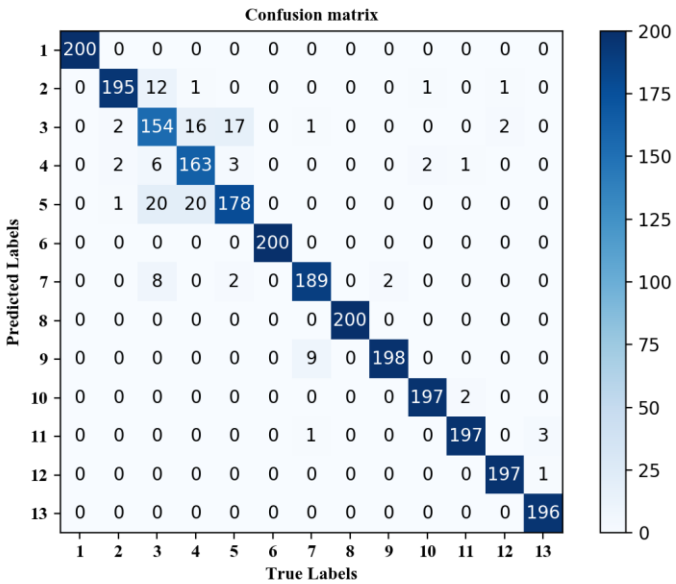

Figure 9. Confusion matrix diagram of the T-20 dataset training model.

4. Conclusion

In this paper, a rolling bearing fault diagnosis method based on time-frequency transformation enhanced CL is proposed and evaluated. Large unlabeled samples collected from multiple experiments were dimensionally augmented and merged into color spectrograms using STFT. Additionally, a developed CL network is employed to pre-train the feature weights of ResNet18. This mode, in turn, was subsequently fine-tuned using a few labeled samples, resulting in the final recognition model. Moreover, experimental data was collected from bearing tests, and the result analysis validated its effectiveness, demonstrating better performance in comparison to two other current methods. The main advantage of the proposed method is, it provides a potential solution to the "small sample dilemma" in industrial applications through the synergistic effect of physically driven signal processing and self supervised representation learning, specifically, only a small number of labeled fault samples need to be obtained, and a large number of samples during operation do not require manual labeling, significantly reducing the cost and time of manually labeling fault samples.

In further, to advance the proposed semi-supervised fault diagnosis method, several promising directions could be explored. First, while the current method employs STFT to generate graphical samples, integrating complementary time-frequency analysis techniques can enhance enhance the discriminability of 1D-to-2D data conversion, such as, combining STFT and GAF (Gramian Angular Field) through attention-based fusion mechanisms. Second, optimizing the CL architecture to better adapt to bearing-specific fault features. For example, a multi-scale contrastive loss could enforce similarity across time-frequency representations to capture hierarchical fault patterns. In addition, the robustness of the proposed method under under different operating conditions is worth exploring, validating performance across variable speeds, loads, noise levels, and lubrication states is critical to ensure industrial applicability.

Acknowledgement

We gratefully thank Kumar et al. for their publicly available dataset of bearing faults.

Funding Statement

This research was funded by the Science and Technology Plan Project of Jiaxing in China (Grant. 2024AY10010), and the Research Projects of Zhejiang Provincial Department of Education in China (Grant. Y202354102).

References

1. Wang X.B., Yao Y.F., Gao C. Wasserstein Distance- EEMD Enhanced Multi-Head Graph Attention Network for Rolling Bearing Fault Diagnosis Under Different Working Conditions. Eksploatacja i Niezawodność – Maintenance and Reliability 2024, 26(2), 184037.
2. Xiao, Y.M., Shao, H.D., Yan, S., et al. Domain generalization for rotating machinery fault diagnosis: A survey. Advanced Engineering Informatics, 2025, 64, 103063.
3. Hei Z.D., Sun W.F., Yang H.Y., et al. Novel Domain-Adaptive Wasserstein Generative Adversarial Networks for Early Bearing Fault Diagnosis under Various Conditions. Reliability Engineering and System Safety, 2025, 257, 110847.
4. Yan S., Shao H.D., Wang J., et al. LiConvFormer: A lightweight fault diagnosis framework using separable multiscale convolution and broadcast self-attention. Expert Systems with Applications, 2024, 237, 121338.
5. Kumar A. Research overview and prospect in condition monitoring of compressors. Expert systems with applications, 2025, 277, 127284.
6. Li X., Cheng J., Shao H.D., et al. A fusion CWSMM-based framework for rotating machinery fault diagnosis under strong interference and imbalanced case. IEEE Transactions on Industrial Informatics, 2021, 18(8): 5180-5189. https://doi.org/10.1109/TII.2021.3125385
7. Yin, H., Wang, Y., Sun, W., et al. Fault diagnosis of hydraulic system based on D-S evidence theory and SVM. International Journal of Hydromechatronics, 2024, 7(1): 1-15. https://doi.org/10.1504/IJHM.2024.135976
8. Xiao, Y.M., Shao H.D., Yan, s., et al. Domain generalization for rotating machinery fault diagnosis: A survey. Advanced Engineering Informatics, 2025, 64, 103063.
9. Hei Z.D., Yang H.Y., Sun W.F., et al. Multiscale Conditional Adversarial Networks based domain- adaptive method for rotating machinery fault diagnosis under variable working conditions, ISA Transactions, 2024, 154: 352-370. https://doi.org/10.1016/j.isatra.2024.08.027
10. Jing, C., He, X., Xu, G.C., et al. Finite Element ModelingAssisted Deep Subdomain Adaptation Method for Tool Condition Monitoring. Processes 2025, 13, 545. https://doi.org/10.3390/pr13020545.
11. Xi, C., Yang, J., Liang, X., et al. An improved gated convolutional neural network for rolling bearing fault diagnosis with imbalanced data, International Journal of Hydromechatronics, 2023, 6(2): 108-132.
12. Kumar A., Kumar R., Xiang J.W., et al. Digital twin-assisted AI framework based on domain adaptation for bearing defect diagnosis in the centrifugal pump. Measurement, 2024, 235, 115013.
13. Fu Y.D., Zhong M.P., Huang J.F., et al. Denoising diffusion probabilistic model enhanced tool condition monitoring method under imbalanced conditions. Measurement Science and Technology, 2024, 36, https://doi.org/10.1088/1361-6501/ad86d5
14. Zhang, J., Liu, M., Deng, W., et al. Research on electro-mechanical actuator fault diagnosis based on ensemble learning method. International Journal of Hydromechatronics, 2024, 7(2): 113-131. https://doi.org/10.1504/IJHM.2024.138231
15. Anil K. Adam G., Hesheng T., et al. Knowledge addition for improving the transfer learning from the laboratory to identify defects of hydraulic machinery. Engineering Applications of Artificial Intelligence, 2023, 126, 106756.
16. Hei Z.D., Shi Q., Fan X.F., et al. Distance-guided domain adaptation for bearing fault diagnosis under variable operating conditions. Measurement Science and Technology, 2024, 35, https://doi.org/10.1088/1361-6501/ad3c5e
17. Wang S.H., Xiang J.W., Zhong Y, et al. Convolutional neural network-based hidden Markov models for rolling element bearing fault identification. Knowledge-Based Systems, 2018, 144: 65-76. https://doi.org/10.1016/j.knosys.2017.12.027
18. Anil K., Vashishtha G., Gandhi C.P., et al. Novel convolutional neural network (NCNN) for the diagnosis of bearing faults in rotary machinery. IEEE Transactions on Instrumentation and Measurement, 2021, 70: 1-10. https://doi.org/10.1109/TIM.2021.3055802
19. Zhao R., Yan R.Q., Wang J., et al. Learning to monitor machine health with convolutional bi-directional LSTM networks. Sensors, 2017, 17(2): https://doi.org/10.3390/s17020273

20. Cao X.C., Chen B.Q., Zeng N. A deep domain adaption model with multi-task networks for planetary gearbox fault diagnosis. Neurocomputing, 2020, 409: 173-190. https://doi.org/10.1016/j.neucom.2020.05.064
21. Zhou Y.Q., Sun B.T., Sun W.F., et al. A tool condition monitoring method based on two-layer angle kernel extreme learning machine and binary differential evolution for milling. Measurement, 2020, 166, 108186.
22. Wang H.C., Sun W., Sun W.F., et al. A novel tool condition monitoring based on Gramian angular field and comparative learning. International Journal of Hydromechatronics, 2023, 6(2): 93-107. https://doi.org/10.1504/IJHM.2023.130510
23. Xiao Y.M., Shao H.D., Lin J., et al. BCE-FL: A Secure and Privacy-Preserving Federated Learning System for Device Fault Diagnosis under Non-IID Condition in IIoT. IEEE Internet of Things Journal, 2024, 11(8): https://doi.org/10.1109/JIOT.2023.3340745
24. Zhu Q.S., Sun B.T., Zhou Y.Q., et al. Sample augmentation for intelligent milling tool wear condition monitoring using numerical simulation and generative adversarial network. IEEE Transactions on Instrumentation and Measurement, 2021, 70, https://doi.org/10.1109/TIM.2021.3077995.
25. Zhou Y.Q, Zhi G.F., Chen W, et al. A new tool wear condition monitoring method based on deep learning under small samples. Measurement, 2022, 189: 110622.
26. He X., Zhong M.P., He C., et al. A Novel Tool Wear Identification Method Based on a Semi-Supervised LSTM. Lubricants 2025, 13, 72. https://doi.org/10.3390/lubricants13020072
27. Zhou Y.Q., Wang H.C., Wang G.H., et al. Semi-Supervised Multiscale Permutation Entropy- Enhanced Contrastive Learning for Fault Diagnosis of Rotating Machinery. IEEE Transactions on Instrumentation and Measurement, 2023, 72, https://doi.org/10.1109/TIM.2023.3301051
28. Hadsell R., Chopra S., LeCun Y. Dimensionality reduction by learning an invariant mapping [C] // 2006 IEEE Computer Society Conference on Computer Vision and Pattern Recognition (CVPR'06). IEEE, 2006, 2: 1735-1742. https://doi.org/10.1109/CVPR.2006.100
29. Chen T., Kornblith S., Norouzi M., et al. A simple framework for contrastive learning of visual representations [C] // International conference on machine learning. PMLR, 2020: 1597-1607.
30. Xia X., Yin H., Yu J., et al. Self-supervised hypergraph convolutional networks for session-based recommendation[C]//Proceedings of the AAAI conference on artificial intelligence. 2021, 35(5): 4503-4511. https://doi.org/10.1609/aaai.v35i5.16578
31. Wu Z., Wang S., Gu J., et al. Clear: Contrastive learning for sentence representation. arXiv preprint arXiv, 2020, 2012.15466.
32. Zhang D., Nan F., Wei X., et al. Supporting clustering with contrastive learning. arXiv preprint arXiv, 2021, 2103.12953.
33. Chen X., He K. Exploring simple siamese representation learning[C]//Proceedings of the IEEE/CVF Conference on Computer Vision and Pattern Recognition. 2021: 15750-15758. https://doi.org/10.1109/CVPR46437.2021.01549
34. Aafaq N., Akhtar N., Liu W., et al. Spatio-temporal dynamics and semantic attribute enriched visual encoding for video captioning[C]//Proceedings of the IEEE/CVF Conference on Computer Vision and Pattern Recognition. 2019: 12487-12496. https://doi.org/10.1109/CVPR.2019.01277
35. Chin C.H., Abdullah S., Singh S.S.K., et al. Strain generation for fatigue-durability predictions considering load sequence effect of random vibration loading. International Journal of Fatigue, 2023, 166, 107242.
36. Hamzi N.M., Singh S.S.K., Abdullah S., et al. Characterising Multiaxial Fatigue Random Strain Time Domain in Assessing the Durability of a Suspension Coil Spring. Experimental Techniques, 2023, 47(3): 655-667. https://doi.org/10.1007/s40799-022-00578-1
37. Firdous A.S., Waseem Z.L., Azhar Y.T. Short-time quadratic-phase Fourier transform. Optik, 2021, 245, 167689
38. Kumar A., Zhou Y.Q., Gandhi C.P., et al. Bearing fault size assessment using wavelet transform based Deep Convolutional Neural Network (DCNN). Alexandria Engineering Journal, 2020, 59(2): 999-1012. https://doi.org/10.1016/j.aej.2020.03.034